Available online at www.sciencedirect.com
ScienceDirect
Journal of Magnetic Resonance 183 (2006) 41–49
JMR Journal of Magnetic Resonance
www.elsevier.com/locate/jmr

Encoding to the longitudinal magnetization for MR imaging and flow velocity mapping

Jung-Jiin Hsu *,[1], Irving J. Lowe

Department of Physics and Astronomy, University of Pittsburgh, Pittsburgh, PA 15260, USA
Pittsburgh NMR Center for Biomedical Research, Carnegie Mellon University and University of Pittsburgh, 4400 Fifth Avenue, Pittsburgh, PA 15213, USA

Received 26 April 2006; revised 18 July 2006
Available online 10 August 2006

Abstract

Phase-encoding to the longitudinal magnetization is implemented by adding encoding gradient pulses in the evolution period τ of the NMR pulse sequence 90°_{+x}–τ–90°_{-x}. This work focuses on the effect of the spin–lattice relaxation and its removal and on the constraint that the 90°_{-x} pulse can only transform the phase of the transverse magnetization partially to the longitudinal magnetization. Theoretical analysis shows that the encoded phase information and the spin–lattice relaxation effect are separable and the latter is identical in each repetition in collecting phase-encoding data. Thus the relaxation effect can be eliminated by subtracting a second data set whose phase information is inverted or by alternating the polarity of the relaxation contribution. From data with partial phase information, Fourier-transform image reconstruction results in mirror aliasing in which the two halves of the Fourier spectrum of positive and negative coordinates overlap. Removal of mirror aliasing requires imaging data of the orthogonal component. Nevertheless mirror aliasing is not necessarily a problem, depending on the subject of study. Phase-encoding to the longitudinal magnetization for spatial MRI and flow velocity mapping are demonstrated using the rotating ultra-fast imaging sequence (RUFIS).

Keywords: Longitudinal magnetization; Cosine/sine phase encoding; Velocity mapping; Spin–lattice relaxation; Mirror aliasing; RUFIS

1. Introduction

Consider the NMR pulse sequence 90°_{+x}–τ–90°_{-x}. Suppose that the magnetization is in the longitudinal direction initially. The first 90°_{+x} radio-frequency (RF) pulse turns the magnetization into the transverse plane. After a delay of time τ, the 90°_{-x} RF pulse turns the y, or the cosine component of the transverse magnetization back to the longitudinal direction. The state of the transverse magnetization at the end of the period τ is transformed or partially transformed to the longitudinal magnetization.

Through manipulating the transverse magnetization during the period τ, the triplet 90°_{+x}–τ–90°_{-x} is commonly utilized to prepare the initial state of the longitudinal magnetization M_0 for a succeeding pulse sequence (see, for example, Ref. [1] and references therein). For example, M_0 can be made transverse-relaxation-time weighted by adjusting the length of τ [2–4], or made diffusion weighted by including diffusion sensitive field-gradient pulses in τ [5–8]. Pulse-sequence module for slice selection can be added in τ so that M_0 is not zero only in the desired slice [9]. If phase dispersion is introduced in τ, for example, as deposited by the read-encoding gradient, application of an RF pulse and a read gradient after the 90°_{-x} pulse can induce a stimulated echo [10], which can be utilized for imaging [11]. The state transformed into the longitudinal magnetization is stored therein and thus can be immune to undesired dephasing caused by such as the eddy current [6]. Motion sensitive studies can also benefit; for example, diffusiveness encoded during a particular phase of the cardiac cycle can be stored and then be recalled by applying an RF

* Corresponding author. Present address: Lucas Center for Imaging, Stanford University, 1201 Welch Road MC 5488, Stanford, CA 94305-5488, USA. Fax: +1 650 723 5795.
E-mail address: jjhsu@stanford.edu (J.-J. Hsu).
[1] Also known as Jason Hsu.

1090-7807/$ - see front matter © 2006 Elsevier Inc. All rights reserved.
doi:10.1016/j.jmr.2006.07.016

pulse at the same phase of the next cardiac cycle so encoding and signal acquisition for a given slice are performed at the same slice location [12,13].

This work explores the utilization of the triplet for phase-encoding to the longitudinal magnetization, which is of interest because, besides preserving the magnetization against dephasing and motion, it adds a dimension to the base imaging pulse sequence following the triplet. This work focuses on resolving two crucial issues: (i) the effect of the spin–lattice relaxation, which distorts the encoding and is often not negligible [4,14], and (ii) the constraint that the phase of the transverse magnetization can only be transformed partially into the longitudinal magnetization. Spatial MRI and flow velocity mapping are demonstrated.

In this paper, the RF pulse which turns the transverse magnetization into the longitudinal direction is termed the *storage pulse*. This pulse is also called driven-equilibrium pulse when meant to rapidly reestablish the equilibrium for samples of long spin–lattice relaxation time [15–17]; this function is irrelevant in this work.

2. Method

2.1. Pulse sequences

The NMR pulse sequences to demonstrate phase-encoding the longitudinal magnetization are depicted in Fig. 1. Both pulse sequences begin with a preparation sequence and are followed by an imaging data acquisition module. The preparation sequence, which is derived from the triplet $90°_{+x}$–τ–$90°_{-x}$, performs slice selection and phase encoding. In this work, the rotating ultra-fast imaging sequence (RUFIS) [4,9,18–20] is employed for data acquisition. For a given initial longitudinal magnetization M_0, RUFIS acquires two-dimensional imaging data. RUFIS consists of a train of low flip-angle RF pulses each of which recalls the encoded longitudinal magnetization to the transverse plane. The direction of the read-encoding gradient is given by $G_x = G_{\text{read}}\cos\theta$ and $G_y = G_{\text{read}}\sin\theta$. The polar angle θ varies through equally spaced values from pulse to pulse in the domain of $[0,2\pi)$ so the free induction decays (FIDs) are radial samples in the two-dimensional image reciprocal domain (k-space). The RUFIS image is reconstructed from the radial samples by filtered back-projection. The spin-lock pulse (SL) is to dephase the magnetization component not in the y direction [9]. The details of the slice selection and the image reconstruction are given in Refs. [4,20]. The whole pulse sequence is repeated for each phase-encoding step. The final data set is three dimensional.

2.2. Phase encoding

In Fig. 1A for spatial MRI, the 180° RF pulse and the companion gradient select a slab transverse to the z direc-

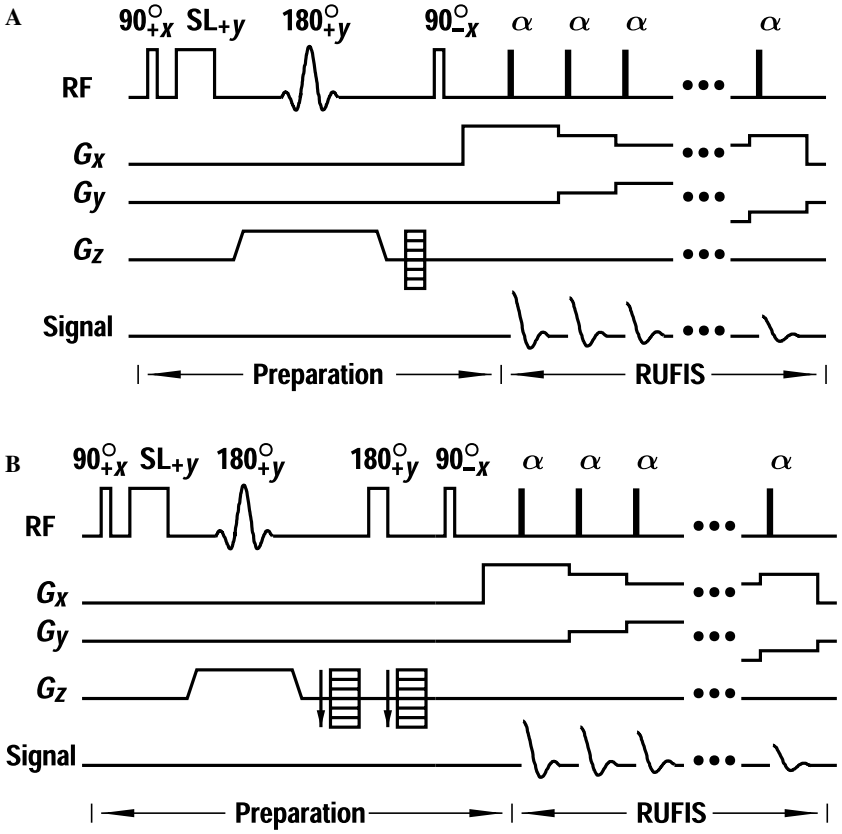

Fig. 1. Example pulse sequences for phase-encoding to the longitudinal magnetization for (A) spatial MRI and (B) velocity mapping. SL is a spin-lock pulse.

tion and the phase encoding is meant to divide the slab into slices by the discrete Fourier transformation. Suppose that, for simplicity, the phase-encoding gradient pulse is rectangular and has time span T_G. The gradient-strength increment ΔG_z between two phase-encoding steps is given by

$$\Delta G_z = -\frac{2\pi}{\gamma Z T_G}, \tag{1}$$

where γ is the gyromagnetic ratio and Z is the desired field of view. In Fig. 1B for velocity mapping, the first 180° RF pulse and the companion gradient select a slab transverse to the z direction and the pair of gradient pulses encodes the velocity. Detailed in Appendix A, the increment ΔG_z is given by

$$\Delta G_z = -\frac{\pi}{\gamma T_V^2 v_{enc}}, \tag{2}$$

where the velocity domain of interest is $[-v_{enc}, v_{enc}]$ and T_V is an effective gradient-pulse time span. A discrete Fourier transformation in the z direction will produce a velocity spectrum in which each image frame is a *velocity slice*. A velocity slice records the distribution of flow particles (i.e., imaginary volume elements of flow) in the slab that travel at the velocity corresponding to that velocity slice. Strictly speaking, the pulse sequence in Fig. 1B encodes only the z component of the velocity vector.

Eqs. (1) and (2) are fundamental in encoding to the transverse magnetization (see, for example, Refs. [21–26]). However, the storage pulse can only turn the cosine component of the transverse magnetization. Cosine is a symmetric function, i.e., $\cos(\phi) = \cos(-\phi)$, so the Fourier transformation will result in aliasing in which the two halves of the spectrum of positive and negative coordinates overlap. The phenomenon is referred to as *mirror aliasing*. Note that if the storage pulse is set at phase $-y$, the sine component is stored. A pulse sequence whose storage pulse stores the cosine component is referred to as *cosine encoding* and the counterpart for the sine component as *sine encoding*. To avoid mirror aliasing, the full phase information needs to be restored; this can be accomplished by combining cosine- and sine-encoding data in the complex number fashion [20,27], i.e., $\cos(\phi) + i\sin(\phi)$, which is demonstrated in Section 3.1. When the mirror aliasing is not a problem, the additional scan for sine encoding is not necessary, which is demonstrated in Section 3.2. Mirror aliasing is elaborated in Section 3.3.

2.3. Spin–lattice relaxation effect

Upon the application of the storage pulse, the magnitude of the longitudinal magnetization represents the encoded phase and starts to evolve towards the thermal equilibrium by the spin–lattice relaxation. In an RF pulse train such as RUFIS (Fig. 1), the NMR signal induced by the ith α RF pulse is proportional to the volume integral of the transverse magnetization $M_{\perp(i)}$ [4]

$$M_{\perp(i)} = \left[M_0 (E_1 \cos\alpha)^{i-1} + M_{eq}(1 - E_1) \frac{1 - (E_1 \cos\alpha)^{i-1}}{1 - E_1 \cos\alpha} \right] \sin\alpha, \tag{3}$$

where $E_1 = e^{-\Delta/T_1}$ with Δ being the pulse spacing, M_0 the initial longitudinal magnetization, α the flip angle, and M_{eq} the equilibrium magnetization. The transverse magnetization is assumed to be fully relaxed before an RF pulse is applied. If the pulse spacing is not uniform, a similar expression can be found in Ref. [28] and the description in this section still applies. In the square brackets in Eq. (3), the first term is referred to as the M_0 *term* or the *decay term* and the second term as the *recovery term*. In Fig. 1, M_0 carries the encoded information. The M_0 term decreases as the time evolves and as the α RF pulses are applied. Thus the signals of the α RF pulses should be normalized by dividing with $(E_1 \cos\alpha)^{i-1}$ to even the contribution of each pulse in the image reconstruction. For fast imaging pulse trains in which $\Delta \ll T_1$ (for example, $\Delta = 220$ μs vs. T_1 of the order of seconds in this work), E_1 can be approximated by unity.

The recovery term increases towards the thermal equilibrium M_{eq}. This term is not a function of M_0; thus it is detrimental to the image accuracy because it does not carry the encoded information but gradually dominates the decreasing M_0 term. When the pulse sequence is repeated to collect imaging data for each phase-encoding step, this term remains the same value in all steps—a signal of zero frequency along the phase-encoding dimension. Consequently, when the Fourier transformation is applied, this term will cumulatively appear and corrupt the slice at the gradient center in spatial MRI or the slice of zero velocity in velocity mapping. Nevertheless accurate results can still be obtained if a second data set is acquired with an inverted initial magnetization $-M_0$. Because the recovery term remains the same, subtracting the two data sets exactly eliminates the recovery term and leaves only the M_0 term with twofold amplitude. In Fig. 1, the sign inversion of the M_0 term can be achieved by setting the phase of the storage pulse to $+x$.

Another technique to deal with the spin–lattice relaxation effect but without the need for the second data set is that, since the recovery term remains constant, if the sign of the recovery term alternates among the phase encoding steps, the Fourier transformation will show the artifact in the most distant slice, leaving the central slice uncorrupted. That is, all the odd (or even) number of phase-encoding steps are executed regularly but all the even (or odd) number of phase-encoding steps are executed with the storage pulse and the receiver phase inverted (i.e., shift the phase by 180°). The sign of the M_0 term remains the same but the sign of the recovery term alternates from step to step.

2.4. Experimental

All of the reported experiments were carried out at 2.35 T with a horizontal-bore superconducting magnet of

31-cm inner diameter and 77-cm length. The NMR probe [20] and the gradient coils were in-house-made. The RF pulse, pre-emphasized gradient outputs, and the Zeeman-field compensation were generated by a programmable digital console. A sinc-shaped RF pulse (5 lobes, truncated at $\pm 3\pi$) was implemented for slice selection. In RUFIS, the read-encoding gradient was 5.5 G/cm and 128 points were sampled for each FID at 1 complex-point per μs; 64 FIDs were acquired for $\theta \in [0,2\pi)$. The α RF pulse spacing was 220 μs. The flip angle was $\alpha = 6^{\circ}{}_{+x}$ or 8 μs.

A gravity-driven flow system was constructed for the velocity-mapping study. Tap water was used and was exposed to the atmosphere overnight prior to the experiment to reduce the bubbles in the fluid. A fluid container was placed 15 cm outside the magnet, or 55 cm from the center of the magnet (also the gradient center). Flow, driven by the gravitational pressure of the fluid, entered into a straight glass pipe through an opening near the bottom of the container. The straight pipe guided the flow horizontally to the center of the magnet. Then the flow was directed to leave the magnet, passed through a flow gauge, and was collected by a reservoir where the fluid was pumped back into the source container. The container had an opening to drain the overflow to maintain constant height of the fluid and therefore constant driving pressure. The flow rate was adjustable by using the flow gauge. In the U-tube experiment, the setup was the same except that a glass U-tube was positioned at the center of the magnet and smoothly connected to the straight inflow pipe. The flow system was similar to the one depicted in Ref. [9] except that flow went directly to the center of the magnet without traveling multiple turns in the magnet; this ensured laminar flow at the location of imaging. Laminar flow is of interest in this work because its theory is well developed.

In this work, the Reynolds number Re of flow was computed by $\mathrm{Re} = \rho v_{\mathrm{avg}} d/\mu$, where ρ is the fluid density, d the diameter of the pipe, μ the viscosity, and v_{avg} the average velocity defined as the volume flow rate divided by the cross-sectional area of the pipe. In this work, $\rho = 1 \times 10^3\ \mathrm{kg/m^3}$ and $\mu = 1 \times 10^{-3}\ \mathrm{N\,s/m^2}$, assuming 20 °C temperature.

3. Results and discussion

3.1. Spatial MRI

An imaging sample was constructed by placing a straight test tube on each side of a U-tube as illustrated in Fig. 2. The glass tubes were filled with distilled water and sealed with rubber stoppers. The sample was positioned such that the target slab was at the center of the gradient and the axes of the tubes were parallel to the direction of the Zeeman field, i.e., the z direction. The sample had uniform density, simple geometry, and gradual change in the cross-section along the axial direction. These features made for easy examination of the result images. In the preparation sequence (cf. Fig. 1A), the central 2.4-cm transverse slab was selected. Sixteen encoding steps were performed. The axial field of view Z was 3.2 cm, slightly wider than the slab width in order to examine the regions inside and outside the slab. Separate scans with the storage pulse set at phase $-x$ and $-y$ were performed to collect the cosine and the sine components of the data, respectively, and the data sets were combined in the complex-number fashion as described in Section 2.2. Scans were also performed with the storage pulse set at phase $+x$ and $+y$ and the data were subtracted from the ones with phase $-x$ and $-y$ to eliminate the spin–lattice relaxation effect as described in Section 2.3.

Fig. 2B shows the 16 slices of the image labeled with their z coordinates relative to the gradient center. The image reflects the sample accurately. The pixel intensity is fairly uniform but the slab thickness is ~0.6 cm less than the 2.4-cm selected owing to the use of a truncated, sinc-shaped RF pulse for the slab selection. Fig. 2C shows the image that is reconstructed without the subtraction of the second data set; the image slice at 0 mm, and only this slice, is corrupted, a unique artifact arising from the spin–lattice relaxation and the Fourier transformation as described in Section 2.3. In the experiment, RUFIS commenced 3 ms after the storage pulse and completed the pulse train in 14.2 ms. Even with such short data acquisition time and a sample of slow relaxation ($T_1 \sim 2$ s), the artifact is noticeable. The four extra bright spots in the 0-mm slice are originated from four pieces of tape adhered axially on the shield of the NMR probe. The tape has relaxation times T_1 and T_2 both less than 1 ms; thus $M_0 \approx 0$ and only the recovery term contributes to the signals.

The second technique to deal with the spin–lattice relaxation effect is to alternate the sign of the recovery term (cf. Section 2.3). The result is shown in Fig. 2D. Since the most distant slice is usually not critical, this alternating scheme sacrifices only one slice but saves the time for acquiring the data to eliminate the spin–lattice relaxation effect.

If only a single scan is performed either for the cosine- or the sine-encoding data set, mirror aliasing will result as discussed in the next section.

3.2. Flow velocity mapping

Consider mapping the axial velocity profile of flow in a straight pipe. In the preparation sequence in Fig. 1B, the central 1-cm slab was selected and 16 velocity encoding steps were performed. For each encoding step, data with the storage pulse set at phase $-x$, $-y$, $+x$, and $+y$ were collected to restore the full encoded phase and to eliminate the spin–lattice relaxation effect. The pipe's inner diameter was 1.9 cm. Four different flow rates were mapped: $v_{\mathrm{avg}} = 0.37$, 1.26, 8.90, and 12.02 cm/s, which corresponded to Reynolds numbers of 70, 240, 1692, and 2283, respectively. For each flow rate, the velocity phase-encoding domain was $[-v_{\mathrm{env}}, v_{\mathrm{env}}]$, where $v_{\mathrm{enc}} = 2.538 v_{\mathrm{avg}}$. The velocity-slice spacing was $0.317 v_{\mathrm{avg}}$ (i.e., $2v_{\mathrm{enc}}/16$ slices). In the resultant

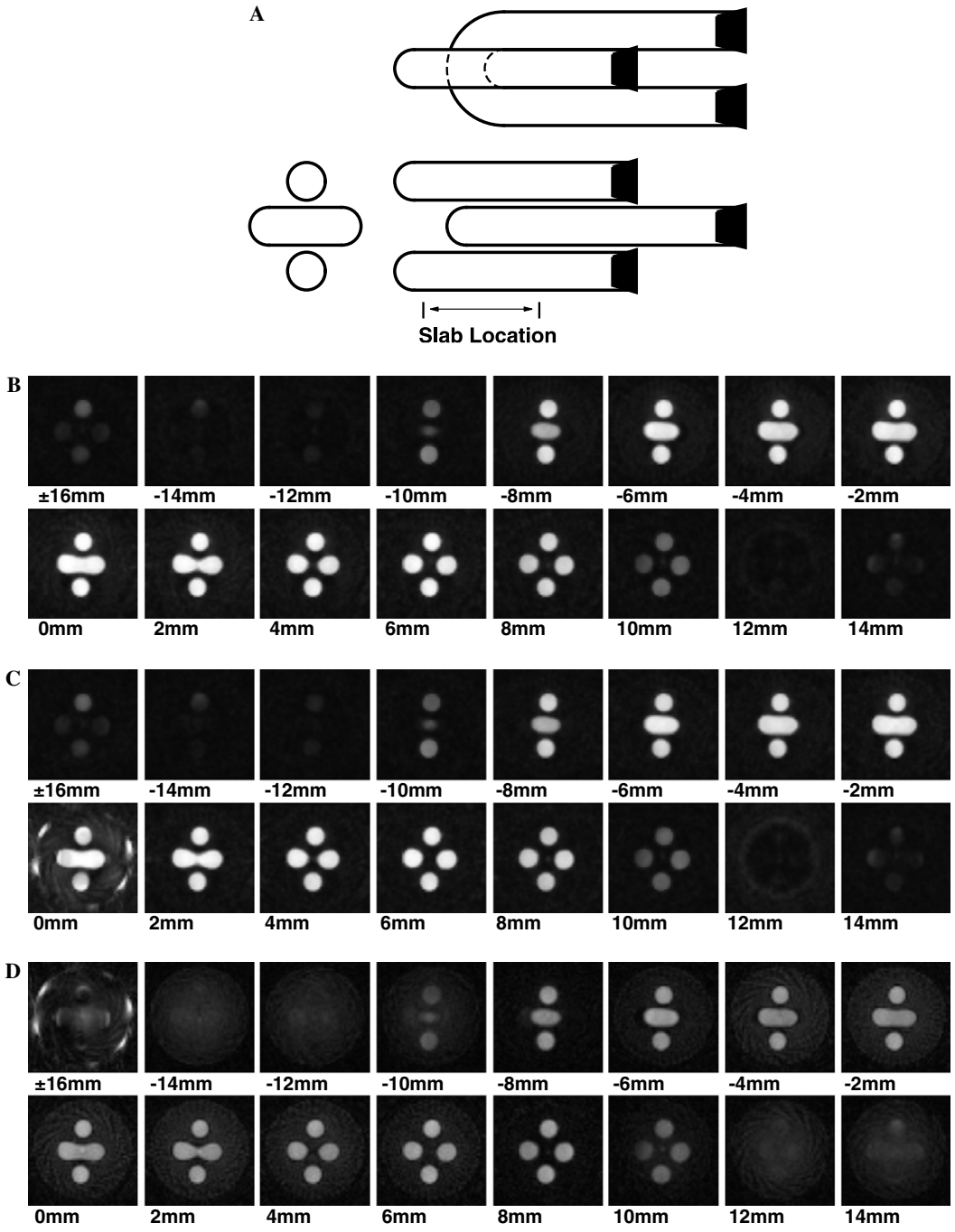

Fig. 2. (A) Orthographic drawing of the imaging sample which consists of a U-tube and two straight tubes; (B) MR image of the sample with the spin–lattice relaxation effect eliminated; (C) MR image without eliminating the spin–lattice relaxation effect; (D) MR image with alternating the recovery term.

velocity spectra, the flow distribution was axially symmetric. Fig. 3 shows the velocity profiles (i.e., the radial coordinate r vs. velocity) constructed by collecting the pixels along a line through the axis in each velocity slice. For better visualization, the pixel intensity is reversed so higher flow particle density is represented by a darker pixel. Since no reverse flow is found (nor is it expected), only the positive velocities are shown. The solid curve is the parabolic profile of well developed laminar flow

$$v(r) = v_{\max}\left[1 - \left(\frac{r}{a}\right)^2\right], \tag{4}$$

where a is the pipe radius. The maximum velocity $v_{\max}$ is $2v_{\text{avg}}$.

The Reynolds numbers experimented for Fig. 3 are in the laminar region [29]; the observation related to this figure is about the *entry length*—the distance downstream from the entry of the pipe required to establish laminar flow. The entry length L can be estimated by [30,31].

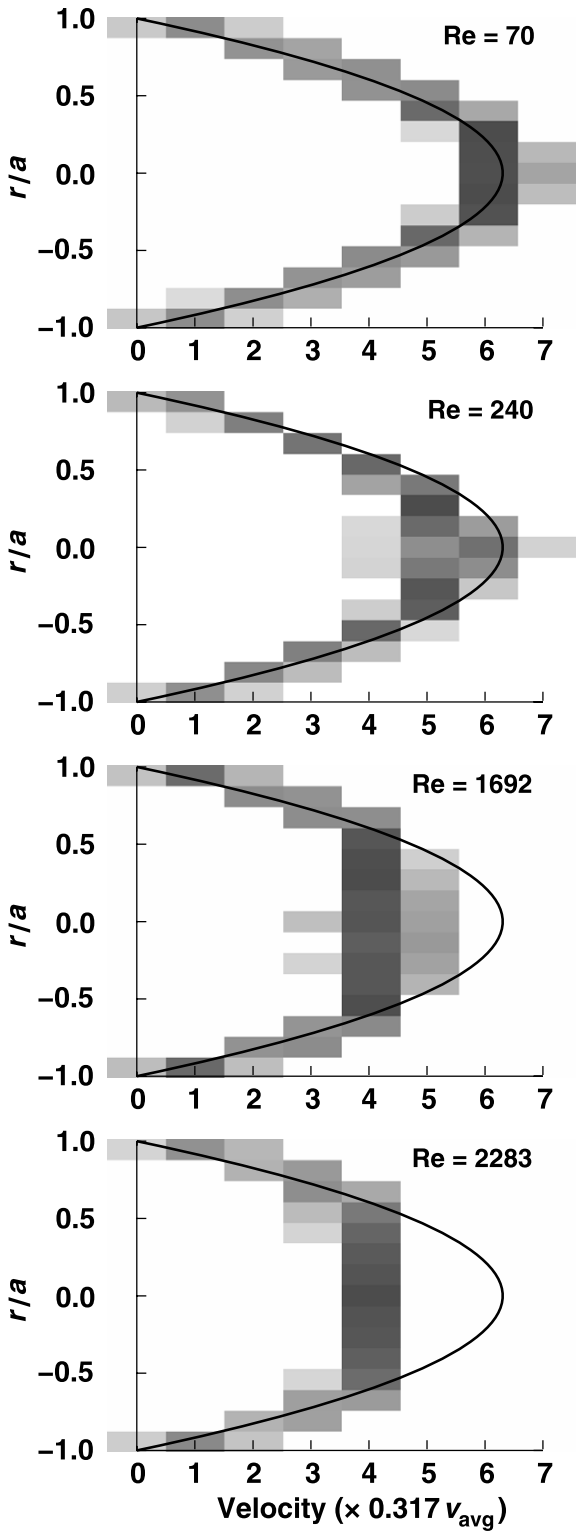

Fig. 3. Velocity profile of flow in a straight pipe of radius a mapped at the same distance from the flow entry. The solid curve is the parabolic profile of well developed lamina flow.

$$L \approx \frac{d\,\mathrm{Re}}{30}. \tag{5}$$

In this work, the distance from the selected slab to the entry of flow is 45 cm; therefore when Re is larger than ~710, the parabolic velocity profile will not be established at the slab. When Re increases, the velocity profile at the slab will evolve effectively as if the slab location moved from the entry length upstream. It is well known that, from the entry length upstream, v_{max} becomes less than $2v_{avg}$ and the velocity profile changes gradually from a paraboloid to a uniform distribution except the layer near the pipe wall [30] (also see, for example, Fig. 2.5 of Ref. [31], Fig. 6.6 of Ref. [29]). This phenomenon is accurately recorded in the mapping as shown in Fig. 3, in which the experimental velocity profile matches the parabola at low Re and becomes uniform at larger Re.

As described in Section 2.2, cosine-encoding alone will result in mirror aliasing. However, mirror aliasing is not a problem for flow systems in which the direction of the velocity is known a priori. For example, in the above experiment on the straight pipe, mirror aliasing does not generate artifact because there is no reverse flow; therefore sine-encoding scans to restore the full phase are not necessary. In the following, mapping with the cosine-encoding alone is demonstrated with flow in a U-tube.

The schematic of the U-tube and the transverse slab locations where the velocity profile were mapped are shown in Fig. 4. The U-tube was made of glass. For each location, the U-tube was positioned such that the target slab was at the gradient center. The slab thickness was 1 cm. There were 17 phase-encoding steps. By using a cosine Fourier transformation computer routine [32], 17 velocity slices were reconstructed. Data sets with the storage pulse set at phase $-x$ and $+x$ were collected to eliminate the spin–lattice relaxation effect. Fig. 4 shows the velocity spectrum for the flow rate of $v_{avg} = 1.07$ cm/s or $\mathrm{Re} = 161$. The velocity encoding domain was $v_{enc} = 2.4$ cm/s. The velocity slices are cropped to an identical region of interest of matrix size 55×24; the pixel intensity is scaled linearly to fit the full gray scale slice by slice. Each velocity slice shows the image of the flow particles traveling at the velocity indicated at the bottom of the figure. For each slab location, the upper row is inflow and the lower row outflow. Three characteristics are of interest. First, since inflow and outflow have opposite signs of velocity but are both shown in the same velocity slices, this experiment is a good example of mirror aliasing. Nevertheless mirror aliasing does not cause any problem since the sign of the velocity is known to the experimenter. Second, the curve of the U-tube makes faster flow particles migrate to the outer wall of the tube owing to the larger centripetal force [33]. This is detected in the mapping: as seen in Fig. 4, at slice locations A and B, the image of outflow in the slices of higher velocity is bent towards the outer wall (i.e., towards the bottom of the figure). Third, the velocity profiles in the inflow leg of the tube and in the outflow leg far away from the U curve are expected to be very similar to that of a straight pipe. Therefore, when the outflow travels from near the curve (location A) through location B and C to D, the velocity profile should develop gradually back to that of the straight pipe, i.e., concentric circles. This is also recorded by the mapping: inflow and outflow profiles are very different in the high velocity slices at location A but the outflow

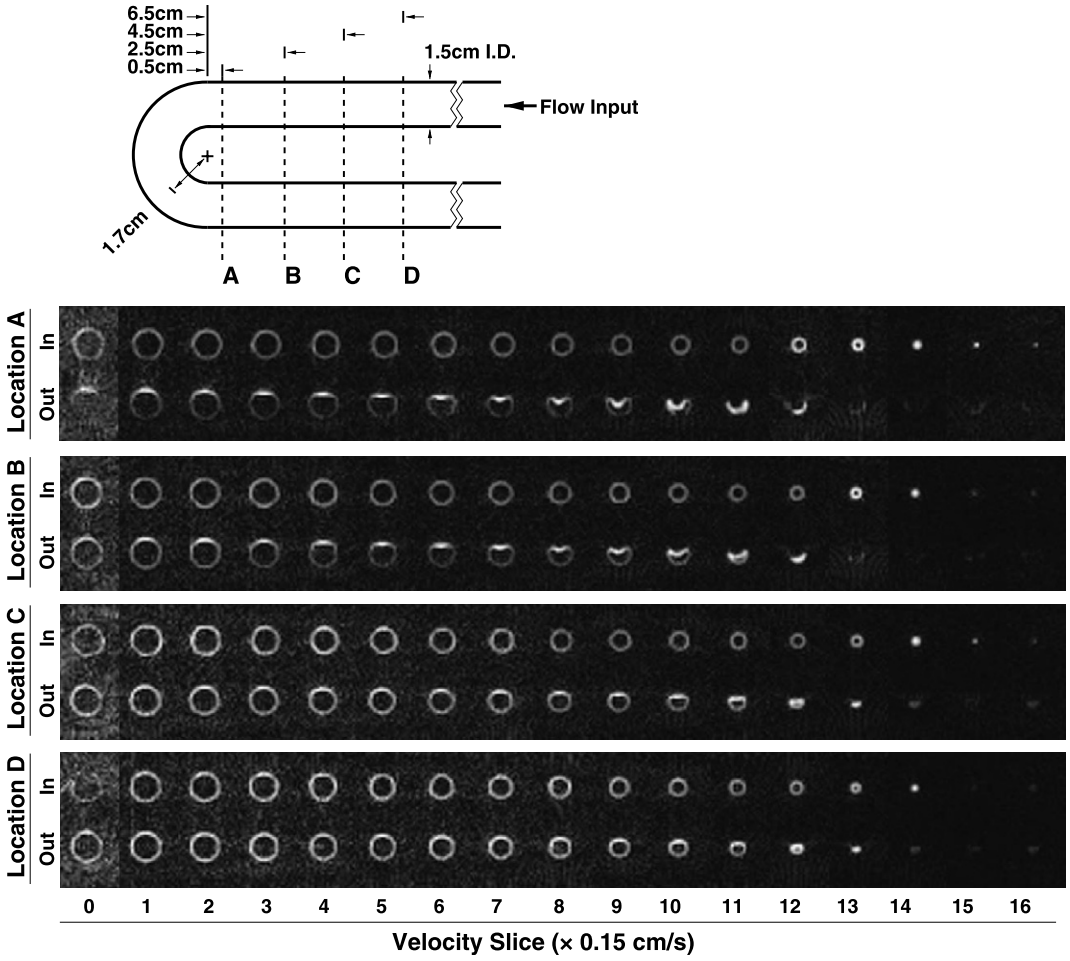

Fig. 4. Schematic (top) and the axial flow-velocity spectra (bottom) of a U-tube. The average flow rate is 1.07 cm/s (Re = 161).

profile changes gradually through location B and C and becomes very similar to the inflow profile at location D.

3.3. Remarks

In Fourier analysis of discrete-time signal, aliasing arises from undersampling. Mirror aliasing, as described in this work, does not relate to sampling. Take spatial MRI for example. Let $D(x,y,z)$ represent the density of the nucleus of interest. Referred to Fig 1A, the k-space representation of the NMR signal data set is given by

$$S(k_x,k_y,k_z) = A\int D(x',y',z')\cos(k_z z')\mathrm{e}^{\mathrm{i}(k_x x'+k_y y')}\mathrm{d}x'\,\mathrm{d}y'\,\mathrm{d}z', \tag{6}$$

where A is a constant to balance the dimension of the equation. For simplicity, the magnetization relaxations are ignored. The image reconstructed by Fourier-transforming S is

$$I(x,y,z) \equiv \frac{1}{8\pi^3 A}\int S(k_x,k_y,k_z)\mathrm{e}^{-\mathrm{i}(k_x x+k_y y+k_z z)}\mathrm{d}k_x\,\mathrm{d}k_y\,\mathrm{d}k_z, \tag{7}$$

$$= \frac{1}{2\pi}\int D(x,y,z')\left(\frac{\mathrm{e}^{\mathrm{i}k_z z'}+\mathrm{e}^{-\mathrm{i}k_z z'}}{2}\right)\mathrm{e}^{-\mathrm{i}k_z z}\mathrm{d}k_z\,\mathrm{d}z', \tag{8}$$

$$= \frac{1}{2}[D(x,y,z)+D(x,y,-z)]. \tag{9}$$

Thus the image is a mixture of $D(x,y,z)$ and its mirror image along the z direction. The analog for velocity mapping is $I_V(x,y,v_z) = [D(x,y,v_z) + D(x,y,-v_z)]/2$. For sine encoding, the image will be $-\mathrm{i}\,[D(x,y,z) - D(x,y,-z)]/2$ and $-\mathrm{i}\,[D(x,y,v_z) - D(x,y,-v_z)]/2$. If an image is reconstructed from cosine- or sine-encoding data alone, mirror aliasing is not avoidable but is not necessarily a problem as demonstrated by the velocity-mapping examples in Section 3.2, in which $D(x,y,v_z) = 0$ for either $v_z > 0$ or $v_z < 0$.

When the encoding to the longitudinal magnetization is in the read, or frequency, direction, the symmetry of the sine and cosine functions generates a problem similar to mirror aliasing. For example, suppose that phase dispersion $k_0 x$ is deposited in the period τ of the triplet $90°_{+x}$–τ–$90°_{-x}$. A $90°_{+x}$ RF pulse recalls the magnetization back to the transverse plane; optional dispersion $k_1 x$ is applied and then the dispersion is refocused by the read gradient in the x direction. The NMR signal is given by

$$S(k) = A\int D(x,y,z)\left[\frac{\mathrm{e}^{\mathrm{i}(k_0+k_1+k)x}+\mathrm{e}^{\mathrm{i}(-k_0+k_1+k)x}}{2}\right]\mathrm{d}x\,\mathrm{d}y\,\mathrm{d}z, \tag{10}$$

where cosine has been substituted by exponentials. An echo appears at $k = -k_0 - k_1$ and at $k = k_0 - k_1$. Depending on the values of k_0 and k_1 and on the length and the location

in time of the signal acquisition window, both echoes can be recorded with possibility of overlapping and truncation, resulting in artifacts in image reconstruction. A solution is to recombine both cosine and sine components of the dispersion k_0x. This is demonstrated in Ref. [34].

As for the spin–lattice relaxation effect, it should be noted that, even with the recovery term eliminated, the M_0 term, which carries the encoded information, decays exponentially with a time constant T_1.

4. Conclusion

Encoding information to the longitudinal magnetization is of interest because it can prepare the initial magnetization of the succeeding pulse sequence with desired weighting and the encoded information is less prone to dephasing effects than it would be if the magnetization were in the transverse plane. Phase-encoding to the longitudinal magnetization adds one Cartesian dimension to the dimensionality of the base imaging pulse sequence. The encoding is accomplished by manipulating the transverse magnetization during the period τ in the triplet $90°_{+x}$–τ–$90°_{-x}$. However the spin–lattice relaxation soon degrades the encoded information. This work revisits phase-encoding to the longitudinal magnetization with emphasis on the spin–lattice relaxation effect and its removal and on the constraint that the triplet pulse module can only encode partial phase information.

Theoretical analysis shows that the encoded information and the spin–lattice relaxation effect are separable and the latter is identical in each repetition for collecting phase-encoding data. Thus the relaxation effect can be eliminated by subtracting a second data set whose phase information is inverted or by alternating the polarity of the relaxation contribution. From data with partial phase information, Fourier image reconstruction results in mirror aliasing, whose removal requires imaging data of the orthogonal component. Nevertheless mirror aliasing is not necessarily a problem, depending on the subject of study.

Two-dimensional RUFIS combined with phase-encoding to the longitudinal magnetization is effective in three-dimensional MRI and in mapping flow velocity in the laminar region experimented.

Acknowledgment

All the experiments were performed at the Pittsburgh NMR Center for Biomedical Research. The Center is supported by NIH Grant P41RR-03631 from the National Center for Research Resources.

Appendix A

In this appendix, a general formula of the gradient-strength increment ΔG is derived for phase-encoding the velocity with trapezoidal gradient pulses shown in Fig. 5. A useful definite integral is

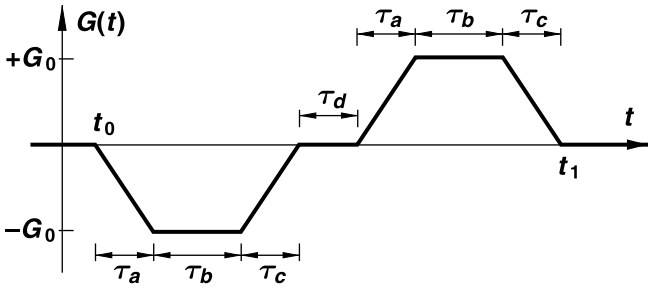

Fig. 5. Trapezoidal, bipolar gradient pulse.

$$\int_{t_0}^{t_0+\tau_a+\tau_b+\tau_c} G(t)t\,\mathrm{d}t = -\frac{1}{6}G_0(3t_0\tau_a + 2\tau_a^2 + 6t_0\tau_b + 6\tau_a\tau_b + 3\tau_b^2 + 3t_0\tau_c + 3\tau_a\tau_c + 3\tau_b\tau_c + \tau_c^2),$$

which can be used to compute for any trapezoidal gradient pulse by substituting proper values for the symbols. Assume that a particle is traveling in the direction of the encoding gradient, e.g., the z direction, at constant velocity v; then $z(t) = z_0 + vt$, where z_0 is the coordinate at time $t = 0$. The angular Larmor frequency related to the gradient is $\omega_L(t) = -\gamma G(t)z(t)$. During the time interval from t_0 to t_1, the particle acquires a gradient-related phase

$$\phi = \int_{t_0}^{t_1} \omega_L\,\mathrm{d}t = -\gamma T_V^2 v G_0,$$

where

$$T_V^2 = \frac{1}{2}(\tau_a^2 + 3\tau_a\tau_b + 2\tau_b^2 + 2\tau_a\tau_c + 3\tau_b\tau_c + \tau_c^2 + \tau_a\tau_d + 2\tau_b\tau_d + \tau_c\tau_d).$$

Therefore the phase difference corresponding to the gradient increment is

$$\Delta\phi = -\gamma T_V^2 v \Delta G.$$

For encoding the domain $[-v_{enc}, v_{enc}]$, replace $\Delta\phi$ by π and v by v_{enc}; then [cf. Eq. (2)]

$$\Delta G = -\frac{\pi}{\gamma T_V^2 v_{enc}}.$$

In this work, the encoding employs a 180° RF pulse and two gradient pulses of the same polarity (Fig. 1); they are effectively the same as the bipolar gradient pulse described here.

References

[1] S.E. Fischer, M. Stuber, M.B. Scheidegger, P. Boesiger, Limitations of stimulated echo acquisition mode (STEAM) techniques in cardiac applications, Magn. Reson. Med. 34 (1995) 80–91.
[2] A. Haase, Snapshot FLASH MRI. Application to T1, T2, and chemical-shift imaging, Magn. Reson. Med. 13 (1990) 77–89.
[3] J.P. Mugler III, T.A. Spraggins, J.R. Brookeman, T2-weighted three-dimensional MP-RAGE MR imaging, J. Magn. Reson. Imaging 1 (1991) 731–737.
[4] J.-J. Hsu, I.J. Lowe, Spin–lattice relaxation and a fast T_1-map acquisition method in MRI with transient-state magnetization, J. Magn. Reson. 169 (2004) 270–278.

[5] H. Lee, R.R. Price, Diffusion imaging with the MP-RAGE sequence, J. Magn. Reson. Imag 4 (1994) 837–842.
[6] U. Sinha, S. Sinha, High speed diffusion imaging in the presence of eddy current, J. Magn. Reson. Imaging 6 (1996) 657–666.
[7] D.L. Thomas, G.S. Pell, M.F. Lythgoe, D.G. Gadian, R.J. Ordidge, A quantitative method for fast diffusion imaging using magnetization-prepared TurboFLASH, Magn. Reson. Med. 39 (1998) 950–960.
[8] U.G. Nolte, J. Finsterbusch, J. Frahm, Rapid isotropic diffusion mapping without susceptibility artifacts: whole brain studies using diffusion-weighted single-shot STEAM MR imaging, Magn. Reson. Med. 44 (2000) 731–736.
[9] H.M. Gach, I.J. Lowe, Characterization of flow emerging from a stenosis using MRI, Magn. Reson. Med. 40 (1998) 559–570.
[10] E.L. Hahn, Spin echoes, Phys. Rev. 80 (1950) 580–594.
[11] J. Frahm, K.D. Merboldt, W. Hänicke, A. Haase, Stimulated echo imaging, J. Magn. Reson. 64 (1985) 81–93.
[12] R.R. Edelman, J. Gaa, V.J. Wedeen, E. Loh, J.M. Hare, P. Prasad, W. Li, *In vivo* measurement of water diffusion in the human heart, Magn. Reson. Med. 32 (1994) 423–428.
[13] J. Dou, T.G. Reese, W.-Y.I. Tseng, V.J. Wedeen, Cardiac diffusion MRI without motion effects, Magn. Reson. Med. 48 (2002) 105–114.
[14] J. Coremans, M. Spanoghe, L. Budinsky, J. Sterckx, R. Luypaert, H. Eisendrath, M. Osteaux, A comparison between different imaging strategies for diffusion measurements with the centric phase-encoded turboFLASH sequence, J. Magn. Reson. 124 (1997) 323–342.
[15] E.D. Becker, J.A. Ferretti, T.C. Farrar, Driven equilibrium Fourier transform spectroscopy. A new method for nuclear magnetic resonance signal enhancement, J. Am. Chem. Soc. 91 (1969) 7784–7785.
[16] R.R. Shoup, E.D. Becker, T.C. Farrar, The driven equilibrium fourier transform NMR technique: an experimental study, J. Magn. Reson. 8 (1972) 298–310.
[17] J.H. Maki, G.A. Johnson, G.P. Cofer, J.R. MacFall, SNR improvement in NMR microscopy using DEFT, J. Magn. Reson. 80 (1988) 482–492.
[18] D.P. Madio, I.J. Lowe, Ultra-fast imaging using low flip angles and FIDs, Magn. Reson. Med. 34 (1995) 525–529.
[19] D.P. Madio, H.M. Gach, I.J. Lowe, Ultra-fast velocity imaging in stenotically produced turbulent jets using RUFIS, Magn. Reson. Med. 39 (1998) 574–580.
[20] J.-J. Hsu, I.J. Lowe, Signal recovery in free induction decay imaging using a stimulated spin echo, Magn. Reson. Med. 47 (2002) 409–414.
[21] Z.-P. Liang, P.C. Lauterbur, Principles of Magnetic Resonance Imaging: A Signal Processing Perspective, IEEE Press, New York, NY, 2000.
[22] A. Caprihan, E. Fukushima, Flow measurements by NMR, Phys. Rep. 198 (1990) 195–235.
[23] R. Turner, P. Keller, Angiography and perfusion measurements by NMR, Progr. NMR Spectrosc. 23 (1991) 93–133.
[24] J.M. Pope, S. Yao, Quantitative NMR imaging of flow, Concepts Magn. Reson. 5 (1993) 281–302.
[25] N.J. Pelc, F.G. Sommer, K.C.P. Li, T.J. Brosnan, R.J. Herfkens, D.R. Enzmann, Quantitative magnetic resonance flow imaging, Magn. Reson. Q 10 (1994) 125–147.
[26] E. Fukushima, Nuclear magnetic resonance as a tool to study flow, Annu. Rev. Fluid Mech. 31 (1999) 95–123.
[27] J.-J. Hsu, I.J. Lowe, Spatial three dimensional imaging using RUFIS, in: Proc. Int. Soc. Magn. Reson. Med., Vol. 8, International Society for Magnetic Resonance in Medicine, 2000, p. 680.
[28] J.-J. Hsu, G.H. Glover, Rapid MRI method for mapping the longitudinal relaxation time, J. Magn. Reson. 181 (2006) 98–106.
[29] F.M. White, Fluid Mechanics, third ed., McGraw-Hill, New York, NY, 1994.
[30] A.M.O. Smith, Remarks on transition in a round tube, J. Fluid Mech. 7 (1960) 565–576.
[31] D.J. Tritton, Physical Fluid Dynamics, second ed., Oxford University Press, New York, NY, 1988.
[32] W.H. Press, S.A. Teukolsky, W.T. Vetterling, B.P. Flannery, Numerical Recipes in C: The Art of Scientific Computing, second ed., Cambridge University Press, Cambridge, UK, 1992.
[33] S.A. Berger, L. Talbot, L.-S. Yao, Flow in curved pipes, Annu. Rev. Fluid Mech. 15 (1983) 461–512.
[34] F.H. Epstein, W.D. Gilson, Displacement-encoded cardiac MRI using cosine and sine modulation to eliminate (CANSEL) artifact-generating echoes, Magn. Reson. Med. 52 (2004) 774–781.